

Zeldovich pancakes at redshift zero: the equilibration state and phase space properties

Digvijay Wadekar¹ & Steen H. Hansen²

¹*Department of Physics, Indian Institute of Technology Bombay, Mumbai*

²*Dark Cosmology Centre, Niels Bohr Institute, University of Copenhagen, Juliane Maries Vej 30, 2100 Copenhagen, Denmark*
 digvijay.wadekar93@iitb.ac.in, hansen@dark-cosmology.dk

11 November 2021

ABSTRACT

One of the components of the cosmic web are sheets, which are commonly referred to as Zeldovich pancakes. These are structures which have only collapsed along one dimension, as opposed to filaments or galaxies and cluster, which have collapsed along two or three dimensions. These pancakes have recently received renewed interest, since they have been shown to be useful tools for an independent method to determine galaxy cluster masses.

We consider sheet-like structures resulting from cosmological simulations, which were previously used to establish the cluster mass determination method, and we show through their level of equilibration, that these structures have indeed only collapsed along the one dimension. We also extract the density profiles of these pancake, which agrees acceptably well with theoretical expectations. We derive the observable velocity distribution function (VDF) analytically by generalizing the Eddington method to one dimension, and we compare with the distribution function from the numerical simulation.

1 INTRODUCTION

The large-scale structure of the universe as observed in redshift surveys displays a complicated geometry. This complex structure referred to as the “cosmic web”, is characterized by the presence of clusters, filaments, sheets and voids. More than 30 years ago galaxy surveys found evidence of filaments (Gregory et al. 1981) and analyses of modern surveys find hundreds of filaments and pancakes (Costa-Duarte et al. 2011). Numerical simulations complement the observations, and find that sheets (which include walls and pancakes) may occupy over half of the volume (Hahn et al. 2007a).

The structure of the cosmic web is the result of the gravitational growth of the small amplitude primordial density and velocity perturbations. Zeldovich (1970) first suggested the anisotropic nature of gravitational collapse leading to Zeldovich Pancakes, which are formed when an overdense region collapses first along one of its principal axes. The pancake picture was further developed in Arnold et al. (1982) and Shandarin & Zeldovich (1989). Various papers have simulated Zeldovich pancakes under controlled conditions (Fillmore & Goldreich 1984; Teyssier et al. 1998; Binney 2004; Schulz et al. 2013) which typically involve simulations of particles only along a fixed axis perpendicular to the pancake.

The dynamics of pancakes has been studied extensively with large numerical N -body simulations, where pancakes have been observed over the last almost 20 years (Shandarin et al. 1995). The dynamical importance of these sheets, expressed through the mass fraction of sheets in the cosmic

web is rather uncertain, and varies in the range (6% – 36%), while the volume fraction varies from (5% – 54%) (Cauntun et al. 2014; J. E. Forero-Romero et al. 2009; Hoffman et al. 2012; Hahn et al. 2007a; Shandarin, Habib & Heitmann 2012; Aragón-Calvo, van de Weygaert & Jones 2010; Shen et al. 2006; Doroshkevich 1970).

There are several ways of defining whether a structure in the cosmic web is a filament, sheet, void or halo. Often, structures are differentiated on the basis of eigenvalues of the second derivative of the tidal tensor T_{ij} , for a sheet T_{ij} has only one positive eigenvalue. Alternatively the sheets can be defined through the shear tensor, which is a rescaled derivative of the velocity field. (Hahn et al. 2007; J. E. Forero-Romero et al. 2009; Bond et al. 2010; Costa-Duarte et al. 2011; Hoffman et al. 2012). In recent studies, the entire 6 dimensional phase space information is taken into account for recognizing structures (Shandarin, Habib & Heitmann 2012; Abel et al. 2012; Neyrinck 2012; Neyrinck & Shandarin 2012).

Direct observations of pancakes is extremely difficult whereas identifying halos is straight forward. This is due to their planar nature and their low contrast with the background (Aragón-Calvo 2007; Aragón-Calvo, van de Weygaert & Jones 2010; Cauntun et al. 2014). Generally, there is a non uniform mass distribution along the area of the sheet, since most of the sheet mass is located in a few very massive regions whereas many of the remaining regions have very low density with no massive halos in them. Observations of high-density regions in galaxy observations were pioneered 60 years ago (de Vaucouleurs 1953; Abell 1958), and have to-

day led to the detection of hundreds of sheets (Costa-Duarte et al. 2011). All these sheets are, however, based on overdensities in phase-space only, and it has still not been clearly established to which extent the sheets have in fact collapsed along the one dimension only. This is one of the concerns of the present paper, to consider whether such overdensities in phase-space are indeed sheets.

Recently it was shown, that certain pancakes may be useful as tools to measure the mass of massive galaxy clusters (Falco et al. 2014). These pancakes are positioned at 3-10 virial radii from the cluster. The cluster mass is measured by considering the small perturbation to the Hubble flow, which the galaxy cluster will induce on the observable line of sight velocity of the galaxies in the pancake. One thing missing in this analysis is, however, to confirm that the structures used are indeed pancakes. In this paper we will confirm that this is indeed the case.

Another aspect of pancakes are their density profile perpendicular to the pancake. In the papers (Binney 2004; Schulz et al. 2013) it was shown that cold collapse leads to final equilibria that are close to a universal power-law density profile, with an exponent less than $1/2$. Here we have compared the power law density profile for the sheet observed in a cosmological simulation, and we find that the theoretical prediction are in fair agreement with the result from the cosmological simulation, however, with a slightly more shallow central profile.

Observationally, when a pancake is seen face-on, it is not possible to extract the density profile. However, we derive an equivalent to the Eddington method (Eddington 1916; Binney & Tremaine 2008) in one dimension, which in principle may allow one to extract information about the line of sight density profile, by using the observable distribution of velocities.

2 NUMERICAL SIMULATION OF SHEETS

In order to consider the equilibration level of a pancake, we need to extract a real pancake from a cosmological simulation. A series of recent papers (Shandarin, Habib & Heitmann 2012; Abel et al. 2012; Vogelsberger et al. 2008; White & Vogelsberger 2009; Vogelsberger & White 2011) developed powerful cosmological simulation techniques to analyze the evolution of dark matter sheet. In this paper, we have analysed the sheet at a fixed redshift, $z = 0$. We consider a few of the pancakes used in Falco et al. (2014), which are based on the N-body simulation described there (for more details, see (Kravtsov et al. 1997; Gottloeber & Klypin 2008)). These pancakes were used to demonstrate a new method of measuring the cluster mass, but it was not quantified if these were truly sheets (equilibrated along only one dimension) or instead filaments (equilibrated along two dimensions).

The reason for considering these particular pancakes is that they have been found through a detection method, which will work on directly observable data. As observational quantities one uses only the two-dimensional position on the sky and the line of sight velocity. Here we will, however, analyze these structures using all the information available from the numerical simulation.

The pancakes are pointing almost radially from a large galaxy cluster, and lie at a distance of the order 10-40 Mpc

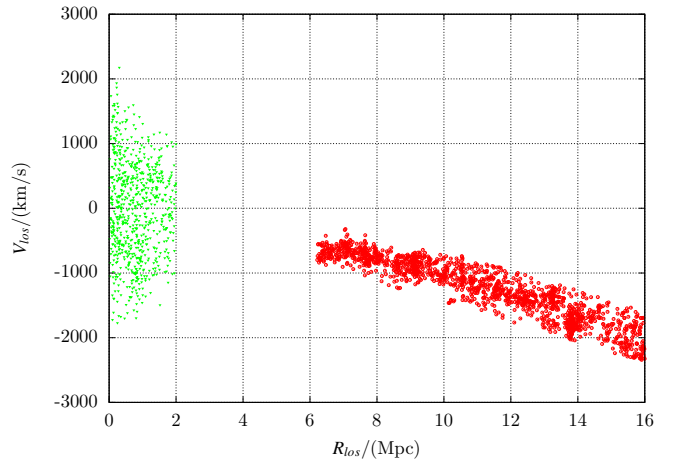


Figure 1. Phase space plot for the extracted sheet. The green points at projected radii smaller than 2 Mpc belong to the central cluster, and the dense, narrow strip between 6 and 16 Mpc is the sheet.

from the cluster. The pancakes are extracted by considering a slice on the sky ($\pi/4$), and then looking for overdensities in the phase-space of projected radius and line of sight velocity, (R, v_{los}) . A sheet produces an almost straight line in that space.

In Figure 1 we show the phase-space plot for the cluster and the extracted sheet. The cluster is a (normal) dense collection of galaxies at projected radii smaller than 2 Mpc, whereas the sheet forms a dense, and fairly narrow strip at projected distances between 6 and 16 Mpc. The velocities are centered at the cluster, and the sheet particles have projected velocities between 500 and 2500 km/sec. Only every 5th point is plotted.

Now, having these sheets, we can rotate them according to their major axes (X,Y,Z), in such a way that X is an axis along the longest axis of the sheet, and Z is an axis along the shortest axis. The latter axis, Z, thus corresponds to the direction perpendicular to the sheet, namely the direction where we anticipate that the collapse has already happened.

This is demonstrated in Figure 2 where we show the real-space projection of the sheet. The x-axis is the distance from the cluster, and we see that the sheet sits in real space at a distance between 10 and 30 Mpc from the cluster. Visually we clearly see, that the sheet is very uniform and broad in the non-collapsed dimension (Y, upper panel), whereas it is much more compact and dense in the collapsed dimension (Z, lower panel).

As a first test, we compare the density profiles along these directions. We confirm that the profile along the Z-direction does appear fairly “gaussian”, whereas the profiles along the other directions (which are expected to not have collapsed yet) are still fairly top-hat shaped, in agreement with the similar findings of (Brinckmann et al 2014).

We also need a selection of galaxies to compare with, a background. For that we consider the same slice on the sky as the signal, however, for the velocity we extract the region with the opposite sign. This means that if the sheet is positioned beyond the cluster (with positive line of sight

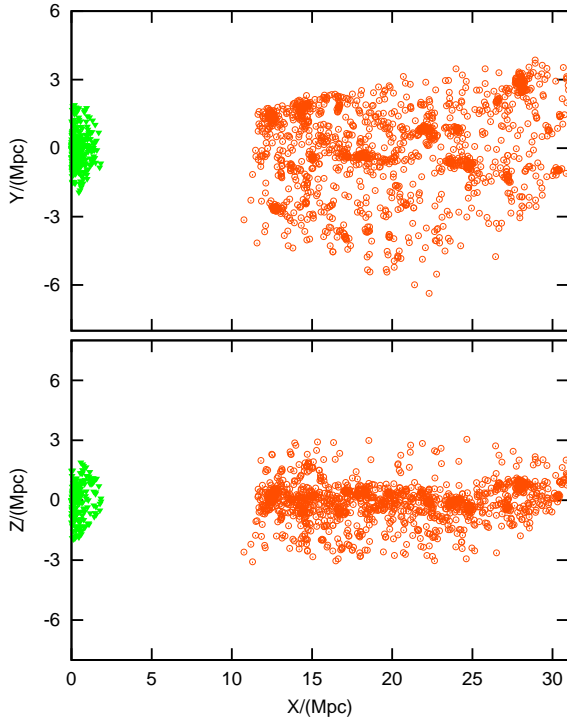


Figure 2. Real space projection of the extracted and rotated sheet. The X-axis corresponds to the distance from the cluster, which is the green points at radius below a few Mpc. The sheet are the red points at distances between 10 and 30 Mpc. We clearly see visually that the one dimension (Z, lower panel) is closer to equilibration than the other dimension (Y, upper panel).

velocity), then the background is selected as the symmetric region, but in front of the cluster (with negative line of sight velocities).

The largest sheet is not a homogeneous box, so we divide it into 10 radial bins (each bin containing equal number of particles) along the X (radial) direction, and the bins are numbered in ascending order of their distance from the cluster. We discard the extreme bins (1 and 10). This may in particular allow us to consider different levels of virialization as a function of distance from the cluster. Similar binning is performed in the background region. We have analysed another two sheets from the numerical simulation. Their properties are qualitatively similar to the sheet discussed in this paper, however, because of a lower number of particles in those sheets, no additional interesting lessons were learned from them.

3 STABILITY ANALYSIS USING PHASE SPACE PLOTS

3.1 Equilibration along different axes

The structure of phase space along different axes can be used to understand the level of equilibration along the particular axes of the structure. For a structure which has reached equilibrium in all the three directions, a phase space plot in

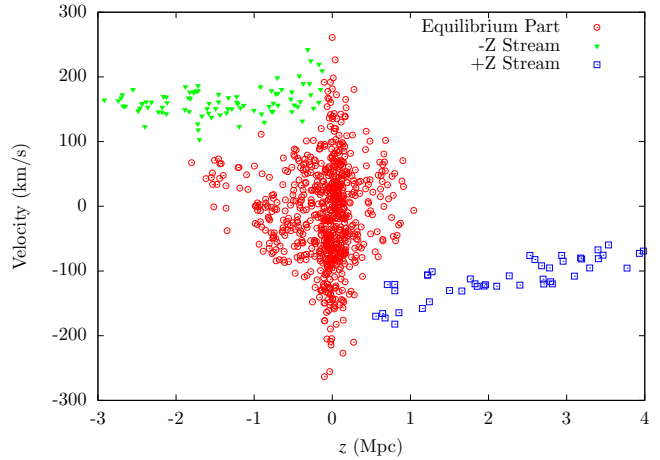


Figure 4. When we remove the Hubble flow, the phase space plot of one radial bin (bin 7) is seen to be divided into an almost equilibrated elliptical part, and 2 infalling streams of galaxies.

any direction will show a semi-gaussian blob. On the contrary, for a structure which remains non-equilibrated along a particular direction, the Hubble flow would completely dominate over the gravitational attraction, and its phase space plot along that direction will show a straight line corresponding to the Hubble expansion.

Phase space plots for one of the radial bins of the largest sheet are shown in figure (3) along with the phase space plots for the background region along the three axes. First of all, the background region (lower panels) is clearly seen to follow the Hubble expansion fairly accurately along all 3 directions. Instead, the signal region (upper panels) clearly shows variation from almost following the Hubble flow (X-direction, right-most panel) to almost being completely equilibrated (Z-direction, left-most panel). The Y-direction is in the early stage of equilibration, only starting to depart from the Hubble flow.

We therefore see, that the sheet candidate indeed is a real 2 dimensional sheet, and therefore differs from a filament, which should be collapsed along 2 dimensions.

A similar analysis for the other radial bins indicate, that the outer bins (6-9) are all in a state which have collapsed along only one dimension, whereas the innermost bins (2-5) are in a more advance state, where either the equilibration has happened along 2 dimensions for some bins, or the presence of substructure is more pronounced. This effect can also be observed by looking at the surface mass density values for the outermost bins(6-9) being $(0.2625 \text{ to } 0.39375) M_{\odot}/pc^2$ which is lower than the density of innermost bins(2-5) which is $(0.4375 \text{ to } 0.875) M_{\odot}/pc^2$. We will therefore limit our analysis to the outermost bins (6-9) for the rest of this paper.

3.2 Phase space structure

In this section we will consider some additional aspects of the phase space plots along the X,Y,Z directions. Considering their dynamic behaviour, the simple Hubble motion of the galaxies is perturbed by the gravitational effect of the cluster

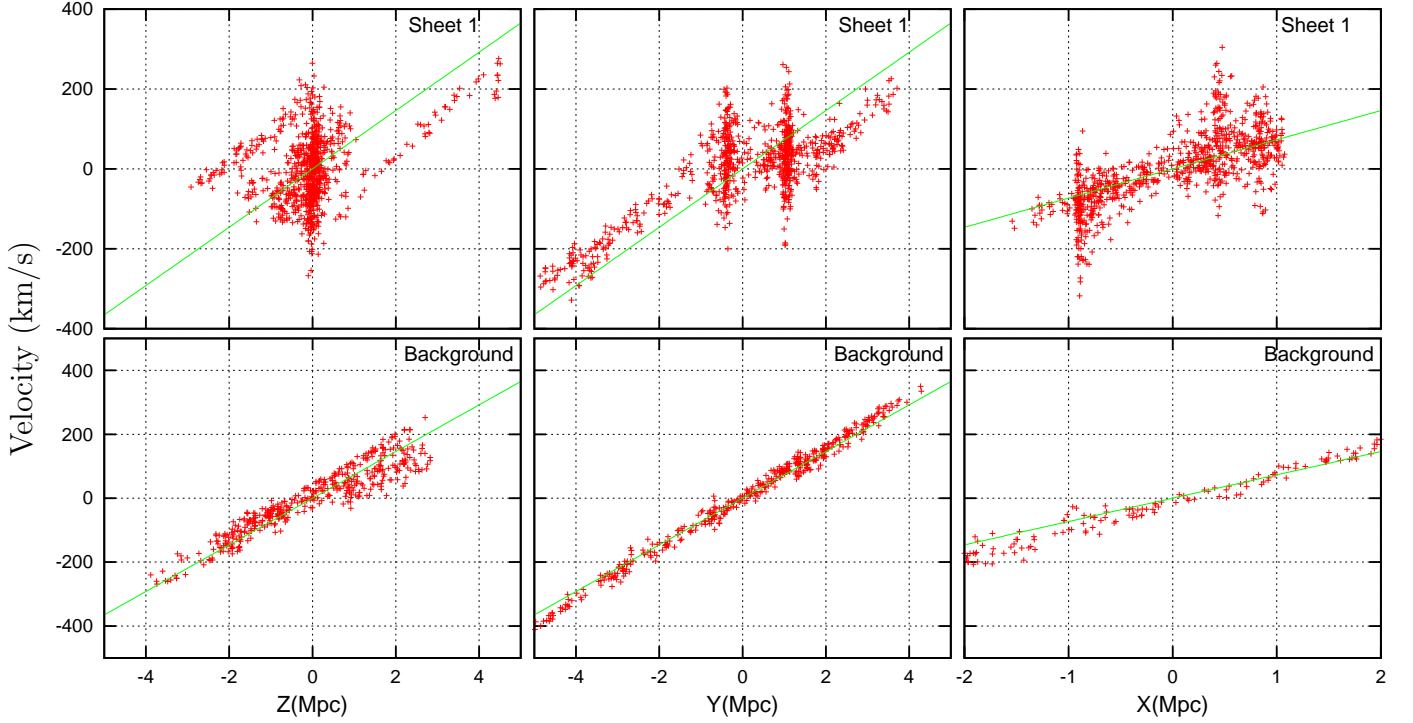


Figure 3. A sheet has been extracted using only observational data, and here we analyse the full phase-space properties of that sheet. The phase space plots for the 7th radial bin of the largest sheet in X,Y,Z directions. The origin of each plot is separately chosen such that mean coordinate and mean velocity of the particular direction are both zero. Also, the Phase Space plots for the background region are provided for comparison. The difference in levels of equilibration along various axes of the sheet is clearly seen. The green line shown in the diagrams represents the Hubble Flow.

mass and the gravitational field of the sheet itself. Thus the total velocity of each particle (galaxy) is the combination of two terms

$$\bar{v}_r(r) = H\bar{r} + \bar{v}_p(r), \quad (1)$$

which are the pure Hubble flow and an infall term v_p . We remind that we have rotated the sheet in such a way, that the X-direction points radially out from the cluster. Considering the motion along the radial X-direction, the corresponding infall term $v_p(x)$ is governed by the gravitational force of the massive nearby cluster (which naturally acts only in the X-direction), and the contribution from the mass of the sheet can be neglected as a first approximation. Outside the region where the Hubble flow starts to dominate, namely outside 3-4 times the virial radius (Prada et al. 2006; Cuesta et al. 2008), the infall term can be approximated to be

$$\bar{v}_p(r) \approx -v_0 \left(\frac{r}{r_v} \right)^{-b}, \quad (2)$$

where r_v is the virial radius and v_0 is an appropriate constant (Falco et al. (2014)). Thus, $\bar{v}_p(r)$ will give the slight deviation from the linear Hubble flow in the slope of the phase space plots in the X-direction for both the sheet and the background regions, seen in the right-most panels in figure 3. For the Y-direction, the sheet has just started to equilibrate, so, deviation caused by the mass of the sheet

itself will be small compared to the Hubble flow, as seen in the middle panel for the sheet.

If we subtract the Hubble flow from the velocity of each particle we obtain the phase space figure (4) for the radial bin 7. This phase-space plot of the perpendicular direction shows the essentially equilibrated central part, and 2 streams of galaxies in the process of falling into the sheet. Each radial bin in the sheet seems to have collapsed into a nearly equilibrated elliptical part and two streams of infalling galaxies which are not part of the virialized structure. We emphasize that only directly observational data was used to identify the sheets (2 position in projected space, and the line of sight velocity), whereas we now, subsequently, consider the full detail of all of phase-space.

By removing the particles in the two streams, we can get the density profile of the equilibrated structure as a function of distance from the center. The profiles are somewhat noisy due to substructures which are not fully equilibrated. The structure of the equilibrated elliptical part in the plots is similar to the plots derived from one dimensional simulations in the paper (Schulz et al. 2013). This is shown in figure (5). We have also plotted a smooth function given by

$$\rho_z(z) \sim |z|^{-\gamma} \exp \left(- \left(\frac{|z|}{z_0} \right)^{1-\gamma} \right), \quad (3)$$

as a fit to the curve. From the fitting curve we find that $\gamma = 0.2$. This can be compared to various analytical predictions:

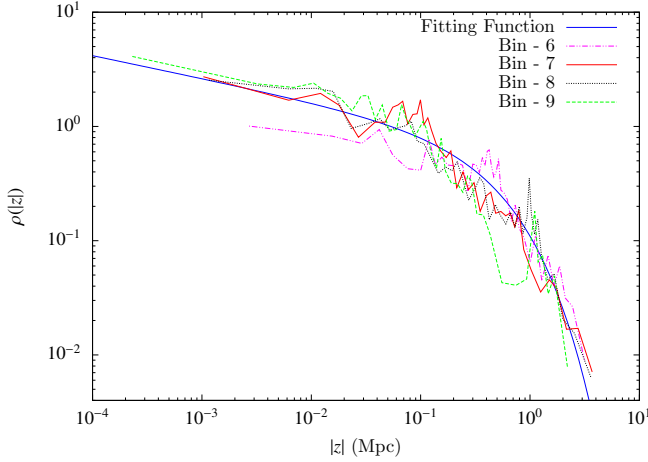


Figure 5. The density profile $\rho(|z|)$ is plotted for the radial bins numbered 6, 7, 8, 9 on a logarithmic scale. The blue fitting curve shows the model in equation (3) with the value of $\gamma = 0.2$

$\gamma = 0.47$ in the paper (Schulz et al. 2013) and $\gamma = 0.5$ in Binney (2004).

3.3 Behavior of Infalling Streams

The streams in figure (4) can be compared to the stages of early equilibration as described in the papers Binney (2004); Schulz et al. (2013). The potential energy of the sheet can be calculated from the density profile using equation (A1). To make a better estimation of the potential energy profile, at distances away from its center, we have taken into account the approximations to be made for a *finite* sheet.

Thus, we have estimated the total energy ($K.E + P.E$) of the infalling particles by comparing the change in kinetic energy of the particles in the 2 streams with the profile of potential energy due to the sheet itself. Energy conservation holds as long as the potential is stable in time. Such a constant total energy curve is given in figure (6). The kinetic energy of particles in both in +Z and -Z streams are compared with the constant total energy curve.

The galaxies in the +Z stream follow this prediction very accurately. The stream on the other side of the sheet clearly has a component of particles (galaxies) which do not follow this simple behaviour. These particles are at distances 1-3 Mpc from the sheet, and have an additional energy of approximately 150 km/sec. In figure 4 we see that these are more dense particles, with a non-zero velocity dispersion. A potential origin of this discrepancy may be related to the non-equilibrated substructures, which are mainly seen in the -Z direction, implying that the -Z stream galaxies could be in a peculiar stage in the equilibration process rather than in a completely free fall motion.

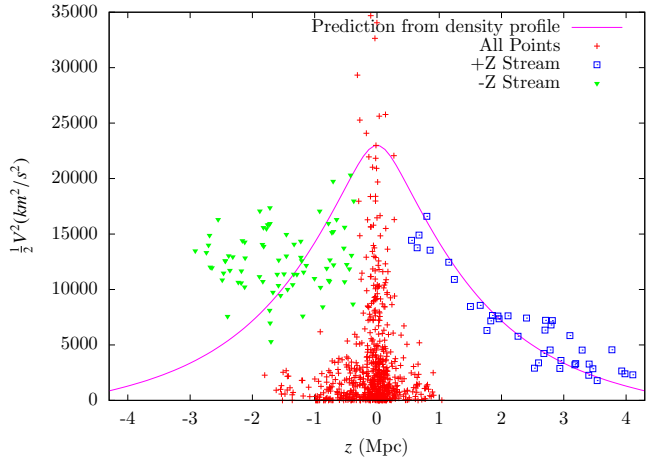


Figure 6. The kinetic energy distribution function $1/2 v_z^2(z)$ of bin 7 are plotted. The fitting function has been derived from the density profile of this bin.

4 EDDINGTON MODEL FOR ONE DIMENSION

In this section, we derive an equivalent of the Eddington model (Eddington 1916; Binney & Tremaine 2008) for its application on isotropic sheets with an infinite area.

We shall consider self-consistent systems in which the density distribution determines the potential through Poisson's equation, and the potential must also determine the density consistently through the collisionless Boltzmann equation.

As we will see, an equivalent of the Eddington model for 3 dimensions can be used approximately for sheets along their perpendicular direction (Z- axis). These sheets are assumed to have uniform spatial distribution along the X-Y plane and to be completely equilibrated along the Z-axis. The change in gravitational potential or the total energy of galaxies along X and Y axis is considered to be negligible as compared to their change along Z axis. Thus we consider only the Z axis values of potential and total energy of the galaxies for our analysis. We define the relative potential Ψ , and the relative energy ξ of a galaxy by

$$\Psi = -\Phi + \Phi_0 \quad \text{and} \quad \xi = \Psi - \frac{v^2}{2} \quad (4)$$

where Φ_0 is a constant such that the conditions $f > 0$ for $\xi > 0$, and $f = 0$ for $\xi \leq 0$ are satisfied.

We can now derive a unique ergodic distribution function (DF) as a function of relative energy $f(\xi)$ from the given density profile of the sheet $\rho(|z|)$ with an infinite extension in the x- and y- direction as

$$f(\xi) = \frac{1}{\sqrt{2\pi}} \int_0^\xi \frac{d\Psi}{\sqrt{\xi - \Psi}} \frac{d\rho}{d\Psi}, \quad (5)$$

where Ψ is the relative potential. The derivation is shown in detail in Appendix-(A), and this result is similar to Eddington (1916).

We can obtain the velocity distribution function $P(v)$

along the line of sight, by integrating $f(\xi)$ as :

$$P(v) = \int_{-z_{\max}}^{z_{\max}} f(\xi) dz \quad (6)$$

where z_{\max} is computed such that $\xi > 0$ is always valid. $P(v)$ is directly observable, and hence this model can in principle be used to extract the density profiles of sheets from the observation of the line of sight velocities of the galaxies belonging to the sheet, even though this practically may never be possible.

5 APPLICATION TO ANALYTICAL MODELS

Let us first consider a few simple and analytical models. We will here assume a known density profile for a sheet and calculate the associated phase space distribution function and velocity distribution function, $P(v)$, using equation (5). The spirit behind this analysis is that direct observations of the sheets give us their velocity distribution function and surface density (Σ) only. The detailed properties of the VDF of the sheets, obtained from the observations, can then be compared to the computed profiles which have the same surface density (Σ) and from it the density profile could be deduced. The analysis in this section is done for idealized sheets with infinite area.

5.1 Model 1 : An Isothermal sheet

First a sheet with a density profile, which is often used in the simulations of the galaxy discs, is examined

$$\rho(z) = \begin{cases} \frac{1}{2a} \Sigma \operatorname{sech}^2\left(\frac{z}{a}\right) & : |z| < z_{\max} \\ 0 & : \text{otherwise} \end{cases} \quad (7)$$

The scale length of the sheet is a , and the value of surface density Σ is normalized such that $2\pi G\Sigma = 1$.

By using equation (5), the phase space distribution function is -

$$f(\xi) = k_1 \int_0^\xi \frac{1}{\sqrt{\xi - \Psi}} e^{-\frac{2}{a}(\Psi_0 - \Psi)} d\Psi \quad (8)$$

$$= k_2 e^{\frac{2}{a}\xi} \operatorname{erf}\left(\sqrt{\frac{2}{a}\xi}\right). \quad (9)$$

Here ‘erf’ represents the error function and k_1, k_2 are normalization constants. The derivation and the approximations involved in calculating Σ are given in the Appendix (B). In order to derive the velocity distribution function.

$$P(v) = k' \int_{-z_{\max}}^{z_{\max}} e^{\frac{2}{a}\left(\Psi - \frac{v^2}{2}\right)} \times \operatorname{erf}\left(\sqrt{\frac{2}{a}\left(\Psi - \frac{v^2}{2}\right)}\right) dz \quad (10)$$

where k' is the constant for normalization, we substitute

$$\Psi = \Psi_0 - a \ln\left(\frac{e^{\frac{\xi}{a}} + e^{-\frac{\xi}{a}}}{2}\right). \quad (11)$$

The definite integral can be computed to get the distribution of velocities. The resulting profile obtained is shown in figure (7) for different values of a .

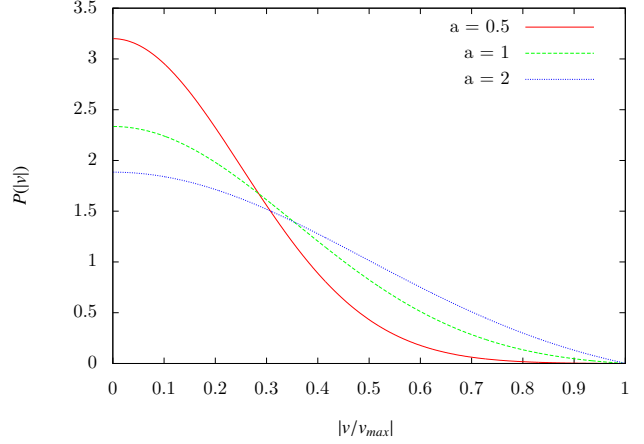


Figure 7. The velocity distribution functions for density profile represented by equation (7) for different values of constant a . The value of mass per unit area (Σ) is kept constant for all the curves.

5.2 Model 2 : A core with a power law cutoff

Another density profile with convenient analytical properties is

$$\rho(z) = \begin{cases} \Sigma \frac{a^2}{2} (z^2 + a^2)^{-\frac{3}{2}} & : |z| < z_{\max} \\ 0 & : \text{otherwise} \end{cases} \quad (12)$$

The scale length of the sheet is a and its surface density is (Σ). The equation for the relative potential becomes

$$\Psi_0 - \Psi = 2\pi G\Sigma(\sqrt{z^2 + a^2} - a) \quad (13)$$

Similar to the previous example, the value of surface density (Σ) is considered such that $2\pi G\Sigma = 1$. The phase space distributions function for two values of a are given below.

5.2.1 $a = 1$

$$f(\xi) = \frac{\sqrt{\xi}}{648(3-\xi)^3} (8\xi^2 - 78\xi + 297) + \frac{5}{8(3-\xi)^{\frac{7}{2}}} \tan^{-1}\left(\sqrt{\frac{\xi}{3-\xi}}\right)$$

5.2.2 $a = 2$

$$f(\xi) = \frac{\sqrt{\xi}}{1536(4-\xi)^3} (8\xi^2 - 104\xi + 528) + \frac{5}{8(4-\xi)^{\frac{7}{2}}} \tan^{-1}\left(\sqrt{\frac{\xi}{4-\xi}}\right)$$

Further, the velocity distribution profile can be obtained by direct integration and resulting profiles obtained are shown in figure (8).

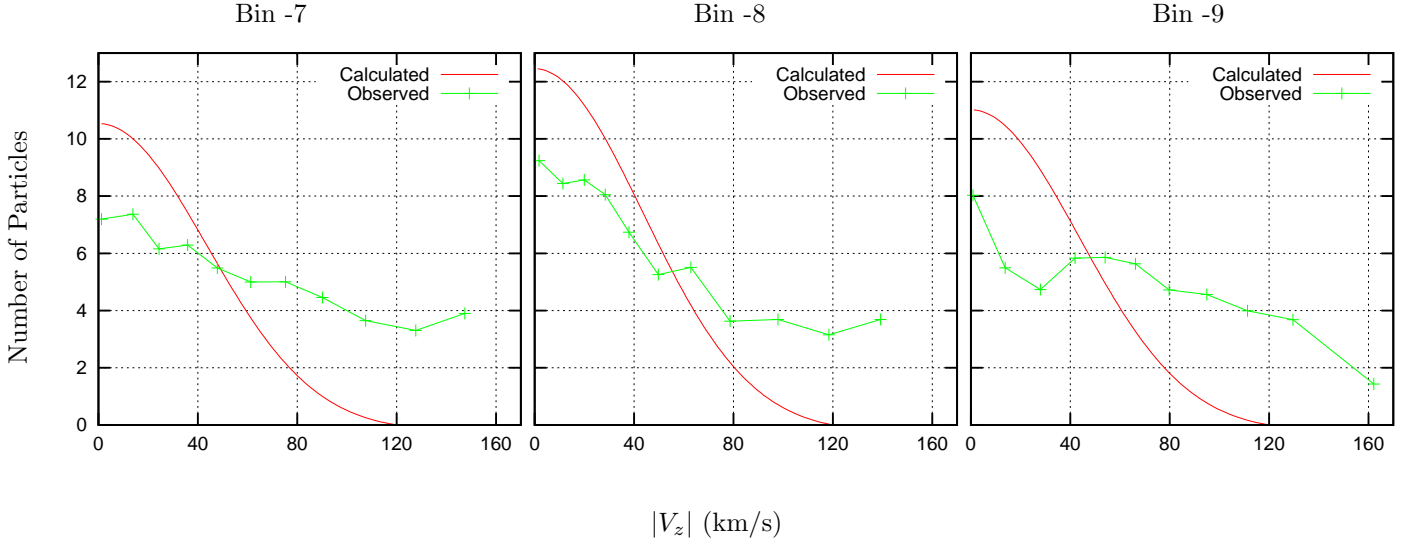


Figure 9. This figure shows the comparison between the observed velocity distribution curves (in green) and the curves derived from the application of Eddington model (in red). The observed velocity distribution curve falls less steeply than the calculated one which implies that the sheet isn't completely equilibrated yet.

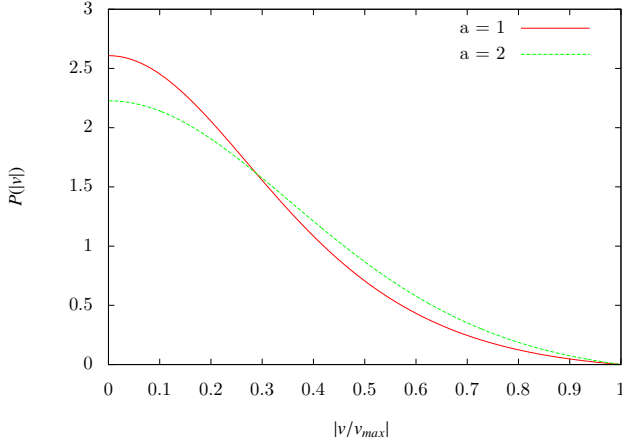


Figure 8. The velocity distribution functions for density profile represented by equation (12) for different values of constant a . The value of mass per unit area (Σ) is kept constant for all the curves.

6 APPLICATION TO SIMULATIONS

In this section we will present a comparison between the derived Eddington Model given by the equation (5) on the simulated CDM sheet described earlier section. We will apply the Eddington formula separately on the 7th, 8th & 9th radial bins of the largest sheet and compare to the analytically calculated velocity distribution curves with the observed VDFs for each of the bins. The calculation is quite tedious due to various approximations and complicated functions are involved in it.

First of all, for the density distribution along the perpendicular axis of the sheet, we will estimate the best-fit parameters for the symmetric analytical model presented in section (5.1). In this step, we have ignored the anisotropies present in the sheet along its perpendicular direction (Z-axis). The gravitational potential function of the sheet is then calculated from the density distribution using the Poisson's equation (A1). In this analysis, we are dealing with particles with z coordinates less than the dimensions of the sheet in the xy plane so we can perform the potential energy calculations similar to the simplified calculation for a sheet of infinite area.

For Eddington formula to be applicable, a structure must be completely equilibrated so that the ergodic hypothesis is valid. The radial bins of the sheet are divided into structures as discussed in section 3.2.

To make a proper comparison between calculated and observed VDFs, we will take into consideration only the particles which lie in equilibrated regions of the sheet for plotting the observed VDF and we will neglect the particles lying in the infalling streams. Using these particles, we can also fix an appropriate value to the width (z_{max}) of the sheet which is an input parameter needed for performing the integration in equation (10).

The computed and observed total velocity distribution curves for each of the bins 7,8,9 are compared separately in the figure (9). The constraints on z_{max} can be used to roughly calculate v_{max} which turns out to be almost 120 km/s in these cases. These curves can be observed to be similar within an order of magnitude. The discrepancies between the calculated and observed VDFs can be attributed to the various approximations which are elaborated in this section.

7 CONCLUSIONS

Zeldovich pancakes are cosmological structures which have collapsed and equilibrated only along the one dimension. These pancakes can be identified at redshift zero using only observational parameters and have recently received renewed interest, since they can be used to measure cluster masses.

We consider the phase-space properties of pancakes from a cosmological numerical simulation, which were detected using the observational technique. We demonstrate how these objects are in the process of equilibrating mainly along the one dimension, and are much less equilibrated along the other two. We extract the density profiles of these structures, and we find fair agreement with theoretical predictions.

ACKNOWLEDGMENTS

It is a pleasure thanking Martina Falco, Radek Wojtak, Martin Sparre, Thejs Brinckmann and Mikkel Lindholmer for discussions. The Dark Cosmology Centre is funded by the Danish National Research Foundation.

REFERENCES

- Abell, G. O. 1958, *ApJS*, 3, 211
 Abel, T., Hahn, O., & Kaehler, R. 2012, *MNRAS*, 427, 61
 Aragón-Calvo M. A., 2007, PhD Thesis, University of Groningen, the Netherlands
 Aragón-Calvo M. A., van de Weygaert R., Jones B. J. T., 2010, *MNRAS*, 408, 2163
 Arnold V. I., Shandarin S. F., Zeldovich Ia. B., 1982, *GapFD*, 20, 111
 Binney J., 2004, *MNRAS*, 350, 939
 Binney J., Tremaine S., *Galactic Dynamics: Second Edition*. Princeton University Press, 2008.
 Bond N. A., Strauss M. A, Cen R., 2010, *MNRAS*, 409, 156
 Brinckmann, T., Lindholmer, M., Hansen, S. H., & Falco, M., 2014, submitted to *MNRAS*.
 Cauntun, M., Waygeart, R., Jones, B. J & Frenk, C. S. 2014, *MNRAS*, 441, 2923
 Costa-Duarte, M. V., Sodr , L., Jr., & Durret, F. 2011, *MNRAS*, 411, 1716
 Cuesta, A. J., Prada, F., Klypin, A., & Moles, M. 2008, *MNRAS*, 389, 385
 de Vaucouleurs, G. 1953, *AJ*, 58, 30
 Doroshkevich A. G., 1970, *Astrophysics*, 6, 320
 Eddington A. S, 1916, *MNRAS*, 76, 572
 Einasto J., Klypin A., Saar E., Shandarin S. F., 1984, *MNRAS*, 206, 529
 Falco M., Hansen S. H., Wojtak K., Brinckmann J. L., Lindholmer, Pandolfi, 2014, *MNRAS*, 442, 1887
 Fillmore J. A., Goldreich P., 1984, *ApJ*, 281, 1
 Forero-Romero J. E., Hoffman Y., Gottlober S., Klypin A., Yepes G. 2009, *MNRAS*, 396, 1815
 Gottlober, S., & Klypin, A. 2008, arXiv:0803.4343 [astro-ph]
 Gregory, S. A., Thompson, L. A., & Tifft, W. G. 1981, *ApJ*, 243, 411

- Hahn O., Carollo C. M., Porciani C., Dekel A., 2007, *MNRAS*, 381, 41
 Hahn O., Carollo C. M., Porciani C., Dekel A., 2007a, *MNRAS*, 375, 489
 Hoffman, Y., Metuki, O., Yepes, G., et al. 2012, *MNRAS*, 425, 2049
 Kravtsov, A. V., Klypin, A. A., & Khokhlov, A. M. 1997, *ApJS*, 111, 73
 Neyrinck M. C., 2012, *MNRAS*, 427, 494
 Neyrinck M. C., Shandarin S. F., 2012, preprint arXiv:1207.4501
 Prada, F., Klypin, A. A., Simonneau, E., et al. 2006, *ApJ*, 645, 1001
 Schulz A. E., Dehen W., Jungman G., Tremaine S., 2013, *MNRAS*, 431, 49
 Shandarin S. F., Melott A. L., McDavitt K., Pauls J. L., Tinker, 2013, *MNRAS*, 431, 49
 Shandarin S. F., Zeldovich Ya. B., 1989, *RvMP*, 61, 185
 Shandarin S., Habib S., Heitmann K., 2012, *Phys. Rev. D*, 85, 083005
 Shen J., Abel T., Mo H. J., Sheth R. K., 2006, *ApJ*, 645, 783
 Teyssier R., Chieze J. P., Alimi J. M., 1988, *ApJ*, 509, 62
 Vogelsberger M., White S. D. M., 2011, *MNRAS*, 413, 1419
 Vogelsberger M., White S. D. M., Helmi A., Springel V., 2008, *MNRAS*, 385, 236
 White S. D. M., Vogelsberger M., 2009, *MNRAS*, 392, 281
 Zeldovich Ia. B., Einasto J., Shandarin S. F., 1982, *Nature*, 300, 407
 Zeldovich Ya. B, 1970, *A&A*, 5, 84

This paper has been typeset from a \LaTeX file prepared by the author.

APPENDIX A: DERIVATION OF ONE DIMENSIONAL EDDINGTON MODEL

This section shows the derivation of an equivalent of Eddington Model for galactic sheets which was earlier presented in equation (10). These isotropic sheets have infinite extension in the x- and y- direction, and are completely equilibrated along their perpendicular dimension with a known density profile $\rho(|z|)$. The Eddington model was originally derived for completely equilibrated three dimensional structures (Eddington 1916; Binney & Tremaine 2008).

We have defined the relative energy and relative potential in equation(4). The relative potential for an isolated system can be calculated using Poisson's equation

$$\Delta\Psi = -4\pi G\rho. \quad (\text{A1})$$

It is possible to derive for the system a unique ergodic distribution function (f) that depends upon the phase-space coordinates only through the Hamiltonian $H(z, v)$ so we can write the DF as a function of the relative energy $f(\xi)$.

The number density $\rho(|z|)$ is an integral of $f(\xi)$ over all velocities. The sheet is completely isotropic thus,

$$\rho(|z|) = 2 \int dv f\left(\Psi - \frac{v^2}{2}\right) \quad (\text{A2a})$$

$$= 2 \int_0^\Psi d\xi \frac{f(\xi)}{\sqrt{2(\Psi - \xi)}}. \quad (\text{A2b})$$

Here we have used the definitions in equation (4) and the value of constant Φ_0 in ξ is chosen such that $\Phi = 0$ and $\xi = 0$ at the boundary of the sheet and $f = 0$ for $\xi \leq 0$. We can write ρ as a function of Φ instead of $|z|$ since Φ is a monotonic function of $|z|$.

$$\frac{\rho(\Psi)}{\sqrt{2}} = \int_0^\Psi d\xi \frac{f(\xi)}{\sqrt{\Psi - \xi}}. \quad (\text{A3})$$

Differentiating both sides with respect to Φ , we obtain

$$\frac{1}{\sqrt{2}} \frac{d\rho}{d\Psi} = \frac{d}{d\Psi} \int_0^\Psi d\xi \frac{f(\xi)}{\sqrt{\Psi - \xi}}. \quad (\text{A4})$$

Note that the integral on the right is the convolution of $f(\xi)$ with $1/\sqrt{\xi}$. Thus taking Laplace transform of both sides

$$\frac{1}{\sqrt{2}} L \left[\frac{d\rho}{d\Psi} \right] = s \times L[f(\xi)] \times L \left[\frac{1}{\sqrt{\xi}} \right]. \quad (\text{A5})$$

Since,

$$L \left[\frac{1}{\sqrt{x}} \right] = \sqrt{\pi} s^{-\frac{1}{2}}, \quad (\text{A6})$$

and on further simplification, we now have an expression for the Laplace transform of $f(\xi)$ in terms of $L \left[\frac{d\rho}{d\Psi} \right]$ as:

$$L[f(\xi)] = \frac{1}{\sqrt{2}\pi} \left(\sqrt{\pi} s^{-\frac{1}{2}} \right) \times L \left[\frac{d\rho}{d\Psi} \right] \quad (\text{A7})$$

Applying the inverted laplace transform on both sides we conclude

$$f(\xi) = \frac{1}{\sqrt{2}\pi} \int_0^\xi \frac{d\Psi}{\sqrt{\xi - \Psi}} \frac{d\rho}{d\Psi}. \quad (\text{A8})$$

This result is similar to (Eddington 1916). It also follows from the equation (A8), that the density distribution for the sheet $v(z)$ in the potential $\Phi(z)$ can arise from an ergodic DF if and only if

$$\int_0^\xi \frac{d\Psi}{\sqrt{\xi - \Psi}} \frac{d\rho}{d\Psi} > 0. \quad (\text{A9})$$

Further to get the velocity profile we need to integrate $f(\xi)$ as :

$$P(v) = k \int_{-z_{\max}}^{z_{\max}} f(\xi) dz \quad (\text{A10})$$

where k is the constant of integration. The range of allowed velocities to keep ξ positive

$$-\sqrt{2\Psi_0} < v < \sqrt{2\Psi_0}. \quad (\text{A11})$$

APPENDIX B: DERIVATION OF THE P(V) CURVE FOR AN ISOTHERMAL SHEET

This section shows the derivation of velocity distribution function for an isothermal sheet which was earlier presented in equation(5). We had used a sheet with a density profile as

$$\rho(z) = \begin{cases} \frac{1}{2a} \Sigma \text{sech}^2\left(\frac{z}{a}\right) & : |z| < z_{\max} \\ 0 & : \text{otherwise} \end{cases}, \quad (\text{B1})$$

where the scale length of the sheet is a , and the surface density is defined as

$$\Sigma = \int_{-z_{\max}}^{z_{\max}} \rho(z) dz \sim \int_{-\infty}^{\infty} \rho(z) dz. \quad (\text{B2})$$

We have used the above approximation considering that z_{\max} is large enough otherwise the value of Σ would depend on value of (a) to keep the value of surface density constant. In the analytical models for sheets the potential along Z axis increases more steeply with distance so to keep the value of Ψ_0 finite we need to constrain z_{\max} to an appropriate value. The relative potential can be calculated as

$$\Psi = \Psi_0 - 2a\pi G \Sigma \ln \left(\frac{e^{\frac{z}{a}} + e^{-\frac{z}{a}}}{2} \right). \quad (\text{B3})$$

We will consider a sheet with the value of Σ normalized such that $2\pi G \Sigma = 1$ to reduce the number of constants. When we use the constraint for $f(\xi)$ being positive, the value of Ψ_0 for $z = 0, v = 0$ is

$$\Psi_0 = \Phi_0 - [\Phi(=0)] = a \ln \left(\frac{1}{2} (e^{\frac{z_{\max}}{a}} + e^{-\frac{z_{\max}}{a}}) \right). \quad (\text{B4})$$

Inverting the coordinate 'z' as a function of Ψ we get,

$$z = a \ln \left(e^{\frac{1}{a}(\Psi_0 - \Psi)} + \sqrt{e^{\frac{2}{a}(\Psi_0 - \Psi)} - 1} \right) \quad (\text{B5})$$

Using the expressions for ρ & Ψ

$$\frac{d\rho}{d\Psi} = \frac{1}{2a^2\pi G} \text{sech}^2\left(\frac{z}{a}\right) \quad (\text{B6})$$

Using the expression in equation (B3) we can use the formula(A8) to obtain

$$f(\xi) = k_1 \int_0^\xi \frac{1}{\sqrt{\xi - \Psi}} e^{-\frac{2}{a}(\Psi_0 - \Psi)} d\Psi \quad (\text{B7})$$

$$= k_2 e^{\frac{2}{a}\xi} \text{erf} \left(\sqrt{\frac{2}{a}\xi} \right) \quad (\text{B8})$$

Here 'erf' represents the error function and k_1, k_2 are normalization constants. Further we substitute back the formula for relative energy from equation (4) to derive the velocity distribution function as

$$P(v) = k' \int_{-z_{\max}}^{z_{\max}} e^{\frac{2}{a}(\Psi - \frac{v^2}{2})} \times \operatorname{erf}\left(\sqrt{\frac{2}{a}(\Psi - \frac{v^2}{2})}\right) dz \quad (\text{B9})$$

where k' is the constant for normalization and we can substitute Ψ from equation (B3). This definite integral is too tedious to compute analytically and can be computed numerically when the values of all variables are provided.